

Functional characterization of a novel CYP119 variant to explore its biocatalytic potential

Tugce Sakalli | Nur Basak Surmeli 

Department of Bioengineering, Faculty of Engineering İzmir Institute of Technology, Urla, İzmir, Turkey

Correspondence

Nur Basak Surmeli, Department of Bioengineering, İzmir Institute of Technology, Fen Fak, A Blok Oda 205, Gülbahçe, Urla, İzmir, Turkey.

Email: nursurmeli@iyte.edu.tr

Funding information

The Scientific and Technological Research Council of Turkey, Grant/Award Number: TUBİTAK, 116Z380

Abstract

Biocatalysts are increasingly applied in the pharmaceutical and chemical industry. Cytochrome P450 enzymes (P450s) are valuable biocatalysts due to their ability to hydroxylate unactivated carbon atoms using molecular oxygen. P450s catalyze reactions using nicotinamide adenine dinucleotide phosphate (NAD(P)H) cofactor and electron transfer proteins. Alternatively, P450s can utilize hydrogen peroxide (H₂O₂) as an oxidant, but this pathway is inefficient. P450s that show higher efficiency with peroxides are sought after in industrial applications. P450s from thermophilic organisms have more potential applications as they are stable toward high temperature, high and low pH, and organic solvents. CYP119 is an acidothermophilic P450 from *Sulfolobus acidocaldarius*. In our previous study, a novel T213R/T214I (double mutant [DM]) variant of CYP119 was obtained by screening a mutant library for higher peroxidation activity utilizing H₂O₂. Here, we characterized the substrate scope; stability toward peroxides; and temperature and organic solvent tolerance of DM CYP119 to identify its potential as an industrial biocatalyst. DM CYP119 displayed higher stability than wild-type (WT) CYP119 toward organic peroxides. It shows higher peroxidation activity for non-natural substrates and higher affinity for progesterone and other bioactive potential substrates compared to WT CYP119. DM CYP119 emerges as a new biocatalyst with a wide range of potential applications in the pharmaceutical and chemical industry.

KEYWORDS

biocatalysis, cytochrome P450, enzyme, monooxygenases, peroxidation, protein engineering

Abbreviations: ABTS, 2,2'-azinobis(3-ethylbenzothiazoline-6-sulfonic acid)-diammonium salt; CAST, combinatorial active-site saturation test; CHP, cumene hydroperoxide; DFSM, dual-functional small molecule; DM, double mutant; DMSO, dimethyl sulfoxide; HRP, horseradish peroxidase; NAD(P)H, nicotinamide adenine dinucleotide phosphate; P450, cytochrome P450; PDB ID, protein data bank identity; RCSB PDB, Research Collaboratory for Structural Bioinformatics Protein Data Bank; REU, Rosetta energy unit; TBHP, *tert*-butyl-hydroperoxide; WT, wild-type.

1 | INTRODUCTION

Cytochrome P450 enzymes (P450s) belong to a superfamily of heme-containing monooxygenases that are involved in the realization of a wide range of biochemical reactions, such as carbon assimilation, biosynthesis of endogenous compounds, as well as xenobiotic detoxification, terpenoids, biodegradation, and drug metabolism.^{1–3} Diversity of biochemical reactions catalyzed by P450s makes them valuable biocatalysts for industrial applications.^{4,5} Especially, the catalysis of regioselective and stereoselective hydroxylation of unactivated carbon atoms by P450s is very important for the chemical and pharmaceutical industry. In this reaction, catalyzed by most P450s, a single oxygen atom of molecular oxygen (O_2) is inserted into an organic substrate using nicotinamide adenine dinucleotide phosphate (NAD(P)H) cofactor as an electron donor. P450s are important biocatalysts for the synthesis of pharmaceuticals due to their roles in many biosynthetic pathways for natural compounds in a wide range of organisms.^{6–8} Indeed, P450s are currently used in the chemical and pharmaceutical industry in the production of drugs and high-value compounds. Some examples of P450 applications are in the production of antibacterial agent erythromycin, statin medication pravastatin (used for lowering blood cholesterol), and steroids like progesterone (used in the treatment of uterine and cervical cancer) and cortisone (used in treatment of allergy and inflammation).⁹ While P450 enzymes have tremendous potentials for industrial applications, there are some limitations in technical implementations of P450s because of the narrow substrate scope of some P450s, low stability, low catalytic efficiency and high cost of cofactors, redox partner and cofactor dependency in industry.^{6,9,10}

Most eukaryotic P450s are membrane bound, unstable, and insoluble in water. P450s act on substrates with low solubility in water, but P450 enzymes show low organic solvent tolerance. Although some eukaryotic P450s shows high substrate promiscuity, these enzymes are not suitable due to membrane-bound for industrial applications. In addition to all these factors, substrate or product toxicity limits P450s' extensive utilization in the industry.¹⁰

Most P450 enzymes require redox partners to transfer electron from the NAD(P)H cofactor for substrate oxygenation. However, electron transfer system is the rate-limiting step of the P450 catalytic cycle in the oxidation reactions. Additionally, expression or isolation of redox partner proteins and the expensive NAD(P)H cofactor increases cost. Uncoupling between NAD(P)H oxidation and product formation results in loss of yield.¹¹ As an alternative to NAD(P)H and molecular oxygen, P450s can also utilize hydrogen peroxide (H_2O_2), through the H_2O_2 -shunt pathway. However, this pathway is very inefficient for most

P450s, except for the P450s in the CYP152 subfamily.^{12,13} In addition, recent studies have shown that the P450 domain of some self-sufficient monooxygenases can also utilize peroxides for generation of drug metabolites.^{14,15} Obtaining soluble and stable P450s that can utilize H_2O_2 has been an appealing target for engineering these enzymes for industrial utilization.^{16,17}

To date, several approaches have been used to increase peroxide-dependent activity of P450s: decoy molecules, dual-functional small molecule (DFSM) co-catalysis, and protein engineering.¹⁸ Decoy molecules can be used to increase substrate promiscuity of CYP152A1 (P450_{BSβ}) to oxidize nonnative substrates using H_2O_2 .¹⁹ DFSMs can act as co-catalysts with an anchoring group for binding to the enzyme, and a basic group to activate H_2O_2 in reactions catalyzed by CYP102A1 (P450BM3).²⁰ Among these strategies, protein engineering acts directly on the catalyst; therefore, it is the most efficient and general way to increase activity with peroxides. Rational design of P450s to increase activity with peroxidases is an ongoing endeavor.^{21–23} However, limited understanding of structural basis for peroxide-supported activity complicates rational design efforts. Joo et al. tried directed evolution of CYP101A1 (P450CAM) to increase its activity of H_2O_2 -driven naphthalene hydroxylation.²⁴ However, characterization of the improved mutant has shown that only trace amounts of hydroxylated naphthalene can be obtained.²⁵

CYP119 is one of the most studied soluble and thermostable P450s; in addition, the crystal structure of CYP119 has been determined by X-ray crystallography.²⁶ CYP119 is obtained from an acidothermophilic bacteria, *Sulfolobus acidocaldarius*, that is known as sulfur-oxidizing organism.^{2,27} *S. acidocaldarius* lives in extreme conditions such as pH 2–4 and at temperatures 78–86°C. Therefore, CYP119 is thermally stable at temperatures of $\leq 85^\circ\text{C}$. Its high stability enables room-temperature experiments in contrast to most P450s.^{28,29} Although redox partners and natural substrates of CYP119 are currently unknown, it has been revealed that CYP119 can oxidize lauric acid using the auxiliary redox partner proteins putidaredoxin and putidaredoxin reductase with NADH as an electron donor.³⁰ CYP119 can also utilize H_2O_2 as an oxidant via the peroxide shunt pathway with low efficiency. Previous studies have demonstrated that CYP119 can catalyze chemical dehalogenation, epoxidation of styrene, hydroxylation of lauric acid, and electrochemical reduction of nitrite, nitric oxide, and nitrous oxide.³¹ Additionally, CYP119 can catalyze the peroxidation of Amplex Red (*N*-acetyl-3,7-dihydroxyphenoxazine) inefficiently in the presence of H_2O_2 .^{23,31,32}

In our previous study, a mutant library of CYP119 was generated by using the combinatorial active-site saturation test (CAST). In the CAST methodology, amino



acid pairs within identified proximity to the active site are randomized pairwise using degenerate codons.³³ This CYP119 mutant library was screened for increased Amplex Red peroxidation activity using a high-throughput assay.³⁴ The novel variant T213R/T214I (double mutant [DM]) CYP119 was obtained from this screen. Isolated DM CYP119 showed five-fold increase in Amplex Red peroxidation activity and two-fold increase in styrene epoxidation activity compared to wild-type (WT) CYP119. The increased peroxidation activity of DM CYP119 utilizing H₂O₂ as an oxidant warrants further biochemical characterization to understand its true potential as an industrial biocatalyst. To this end, here we characterized the activity of DM CYP119 with unnatural substrates like 2,2'-azino-bis(3-ethylbenzothiazoline-6-sulfonic acid)-diammonium salt (ABTS), guaiacol, and investigated its substrate scope using computational analysis. In addition, the stability of DM CYP119 toward peroxides, temperature, and its organic solvent tolerance was investigated and compared to the WT enzyme.

2 | MATERIALS AND METHODS

DM (T213R/T214I) CYP119 was obtained through activity screening of CYP119 mutant library. Expression vector of CYP119 containing the T213R/T214I mutation (pet11a vector + DM CYP119) was obtained from the same library. Expression, isolation, and purification of WT and DM CYP119 were performed as described by previous studies.³⁴ SDS PAGE analysis was performed to assess isolation steps and the purity of the enzymes obtained (Figure S1).

2.1 | UV-visible spectra of WT and DM CYP119

UV-visible spectra of WT and DM CYP119 were analyzed in 50 mM potassium phosphate at pH 7.4 and room temperature. Analysis was performed by 1600PC Scanning Spectrophotometer for the DM CYP119. Deconvoluted peaks and fit components were obtained by Fityk 1.3.1 software by fitting to Gaussian functions with Levenberg-Marquardt method after baseline subtraction.^{35,36}

2.2 | Reactions of WT and DM CYP119 with cumene hydroperoxide (CHP) and *tert*-butyl-hydroperoxide (TBHP)

CHP and TBHP reactions of WT and DM CYP119 were followed by UV-visible spectra. Soret absorbance of WT and DM CYP119 were followed at 414 and 415 nm, respectively. Reaction mixtures included 1.5 mM CHP or TBHP

and 1.5 μM enzyme (WT or DM CYP119) in 50 mM potassium phosphate at pH 7.4. Reaction volume was 700 μl. Potassium phosphate buffer (50 mM) at pH 7.4 was used as blank. The Soret absorbance of WT and DM CYP119 were monitored by following the changes in UV-visible spectra between 350 and 650 nm during the reaction. UV-visible spectra were taken at 0, 2, 5, 10, 20, 30, 45 min after the addition of peroxide. Observed rate constants (k_{obs}) was determined by fitting the data to one-phase exponential decay equation shown in Equation (1), where k is the k_{obs} obtained:

$$y = (y_0 - \text{Plateau}) \times e^{-kx} + \text{Plateau} \quad (1)$$

2.3 | Oxidation activity of DM CYP119

2.3.1 | Guaiacol oxidation reaction with WT and DM CYP119

Guaiacol oxidation reaction was followed in the presence of WT and DM CYP119 at room temperature. Reaction mixtures contained 5 mM guaiacol, 1 mM H₂O₂ and 3 μM enzyme (WT or DM CYP119) in 50 mM potassium phosphate buffer at pH 7.4. Reaction volume was 700 μl. Reaction was initiated by addition of H₂O₂. UV-visible spectra were taken from 350 to 650 nm at 1-min intervals for 20 min. The yield of tetraguaiacol formation is followed by absorbance at 470 nm ($\mathcal{E}_{470\text{nm}} = 2.66 \times 10^4 \text{ M}^{-1} \text{ cm}^{-1}$).³⁷

2.3.2 | ABTS oxidation reaction with DM CYP119

The ABTS oxidation catalyzed by WT and DM CYP119 was monitored at room temperature in 50 mM potassium phosphate buffer at pH 7.4. Reaction volume was 700 μl containing 3 μM enzyme (WT or DM CYP119), 1 mM H₂O₂, and 1 mM ABTS in 50 mM potassium phosphate buffer at pH 7.4. Potassium phosphate buffer (50 mM) was used as blank. Reactions were initiated with addition of 1 mM H₂O₂. The reactions were followed at 1-min intervals from 950 to 350 nm for 45 min. The yield of the ABTS^{•+} radical cation formation by WT and DM CYP119 was assessed by using the extinction coefficient of ABTS^{•+} at 734 nm ($\mathcal{E}_{734\text{nm}} = 1.5 \times 10^4 \text{ M}^{-1} \text{ cm}^{-1}$).^{30,38}

2.4 | Peroxidase activity of WT and DM CYP119 in presence of organic solvents

Organic solvents effects on Amplex Red peroxidation of WT and DM CYP119 were analyzed using 96-well plates. Each well has a total of 100 μl reaction volume containing

H₂O₂ (1 mM), Amplex Red (10 μM), WT CYP119 (1.5 μM), or DM CYP119 (1.5 μM) with different concentrations of organic solvents (0% [positive control] v/v, 2.5% v/v, 5% v/v, 7.5% v/v) in 50 mM potassium phosphate buffer at pH 7.4.

Blank used in the assay was 50 mM potassium phosphate buffer. To control assay whether run or not, positive control was 1 μU horseradish peroxidase (HRP) with H₂O₂ (1 mM) and Amplex Red (10 μM) in 50 mM potassium phosphate buffer at pH 7.4. All components were mixed before adding H₂O₂. After addition of H₂O₂, samples were incubated about 20 min. Fluorescence excited (545 nm) and emitted (595 nm) by resorufin was measured by using FLUOstar Omega (BMG LABTECH).³⁴

2.5 | Peroxidation activity of WT and DM CYP119 based on variable pH

Amplex Red peroxidation reaction of WT and DM CYP119 was analyzed at various pH values. Reaction mixtures contained 1.5 μM enzyme (WT or DM CYP119), 10 μM Amplex Red, 1.5 μM H₂O₂ in a 50 mM potassium phosphate buffer. Each potassium phosphate buffer was prepared at different pH values (5.8, 6.8, 7.4, and 8.0). The resorufin formation was observed at 570 nm during 45 min, with 2-min intervals. The initial rate was calculated for each pH and for 10 min by linear fitting.

2.6 | Thermostability measurements of WT and DM CYP119

Thermostability of WT and DM CYP119 was analyzed by following Soret absorbance with increasing temperature. Enzyme was incubated for 5 min at each temperature (25°C, 40°C, 60°C, 70°C, 75°C, 80°C, 85°C, 90°C, 95°C, respectively) in 50 mM potassium phosphate buffer at pH 7.4. UV-visible spectra for enzyme solutions were monitored for each temperature between 350 and 650 nm. Difference spectra were obtained by subtracting UV-visible spectrum of the enzyme solution at room temperature from the spectra of enzyme at higher temperatures. To make the changes clearer, background subtraction was applied by Fityk 1.3.1. The shift in maximum Soret absorbance was monitored. ΔAbs is defined by the difference of absorbance at the specified wavelength at higher temperature from the absorbance at room temperature.³⁶

2.7 | Docking studies of WT and DM CYP119 with different substrates

Crystal structure of imidazole-bounded WT CYP119 was used for docking studies (protein data bank identity [PDB

ID]: 1F4T).²⁶ First, 1F4T.pdb file was obtained from the Research Collaboratory for Structural Bioinformatics Protein Data Bank (RCSB PDB) database. PyRosetta program was used for docking process. PDB files must be prepared before starting the design process of the PyRosetta program. CleanATOM protocol of PyRosetta was used for removing all heteroatoms and water molecules from .pdb file.³⁹ Then, energy minimization of ligand was done with UCSF Chimera.⁴⁰ Since PyRosetta requires initial coordinates for ligand for docking process, we first performed a dock simulation with UCSF Chimera program. 1F4T.pdb file and minimized ligand were opened on UCSF Chimera. Grid Box (10 × 10 × 5) was formed and placed into the active site of enzyme (1F4T.pdb). Docking of ligand to the enzyme was performed by AutoDock vina. Initial coordinates were obtained for each ligand for using on PyRosetta.

Mutation on the structure of CYP119 was created by the PyRosetta program. The Task Factory module of PyRosetta is used for creation of mutations. Optimization of conformation of mutant residues was performed by the PackRotamersMover function based on the “REF2015” score function. Fast relax method was realized for energy minimization of WT and DM CYP119 structures. “REF2015” score function was used for energy minimization steps. After that ligands were docked with the DockMCMProtocol of the PyRosetta.⁴⁰ One hundred rounds of docking were performed for each ligand for the WT and DM CYP119. Docking protocol that applied on WT and DM CYP119 with various ligands was improved and optimized in our previous work.³⁴ Docking scores of WT and DM CYP119 were calculated for different ligands (guaiacol, Amplex Red, progesterone, phenoxazine, testosterone, indole, indoxylacetate, caffeine, and SDS) with PyRosetta program according to “ligand” score function. The docking results with the lowest Rosetta energy unit (REU) scores were chosen for analysis of ligand–protein interactions. The docking results were visualized by UCSF Chimera software.⁴¹

2.8 | Progesterone binding assay and conversion

Binding constants of WT and DM CYP119 were analyzed at room temperature by difference spectroscopy, utilizing VWR UV/1600PC scanning spectrophotometer. Enzyme solutions were kept for 10 min at room temperature and divided into two glass cuvettes. Progesterone (10, 20, 40, 60, 80, 100, 120, 140, 160 μM) in a dimethyl sulfoxide (DMSO) stock was titrated into the cuvette containing 1.5 μM enzyme (WT or DM CYP119) in 50 mM potassium phosphate buffer at pH 7.4. At the same time, equal volume of DMSO was added into the control cuvette,



respectively. The concentration of DMSO in the cuvette did not exceed 2% of the initial volume. Equal amounts of DMSO were added to the reference cuvette. The absorbance shift between 420 and 388 nm was followed. The shift was plotted against substrate concentration by nonlinear fitting. Value of K_d was calculated by plotting the shift against substrate concentration to quadratic. After incubation for 5 min with substrate, UV spectra were collected between 350 and 650 nm with 1-nm interval for each concentration. The absorbance subtraction between 420 and 388 nm versus concentrations of progesterone were drawn by nonlinear fitting-specific binding analysis in Graphpad. The shift in maximum Soret absorbance was monitored by $\Delta\Delta\text{Abs}$ (420 – 388), where ΔAbs is defined by the difference of absorbance at the specified wavelength at higher progesterone concentrations from the absorbance at zero progesterone concentration. $\Delta\Delta\text{Abs}$ (420 – 388) is obtained by subtraction of $\Delta\text{Abs}_{388\text{ nm}}$ from $\Delta\text{Abs}_{420\text{ nm}}$. The shift was plotted against substrate concentration. The dissociation constant (K_d) was then determined by fitting plots of $\Delta\Delta(420 - 388)$ against substrate concentration to the quadratic equation in Equation (2):

$$\Delta A = \frac{A_{\max}}{[E]} \left(\frac{K_s + [E] + [L] - \sqrt{(K_s + [E] + [L])^2 - 4[E][L]}}{2} \right) \quad (2)$$

To investigate progesterone conversion by DM and WT CYP119, progesterone oxidation reactions were carried out in 500 μl total volume. The reactions contained 10 μM enzyme and 150 μM progesterone and 1 mM CHP in 50 mM potassium phosphate buffer at pH 7.4. The reactions were initiated by addition of CHP and continued for 30 min. They were stopped by addition of 500 μl ethyl acetate. The products were extracted thrice with 1:1 ethyl acetate. The ethyl acetate was evaporated by nitrogen gas. The residues were dissolved in 1 ml methanol and analyzed with high-performance liquid chromatography (HPLC). The HPLC analysis was performed on Agilent 1200 Series by DAD detector. Teknokroma Mediterranea Sea18 RP-C18 (15 \times 0.46, 5 μM) column was used for experiments. The HPLC run started with 40:60 acetonitrile:ddH₂O for 4 min, increasing 100:0 acetonitrile:ddH₂O for 11 min, and 40:60 acetonitrile:ddH₂O for 5 min at flow rate of 1 ml/min. Detection of substrate, oxidant, and products was accomplished by following absorbance at 254 nm.

3 | RESULTS

T213R/T214I (DM) CYP119 is novel mutant of CYP119, which was obtained from a high-throughput screen utilizing Amplex Red peroxidation by a previous study

in our laboratory.³⁴ Initial spectral characterization of DM CYP119 did not display any significant changes in the heme pocket of the enzyme. However, DM showed five-fold higher Amplex Red peroxidation, and two-fold higher styrene epoxidation activity compared to WT CYP119. The increased activity of DM with peroxides and its native thermostability makes it an ideal candidate for industrial biocatalysis. Here, we characterized the substrate scope; stability toward peroxides; temperature and organic solvent tolerance of DM CYP119 to identify its true potential as an industrial biocatalyst.

3.1 | Spectral analysis of WT and DM CYP119

Optical spectra of WT and DM CYP119 were briefly compared in the previous study, and similar spectra were observed for both proteins.³⁴ In this study, background subtraction and Gaussian fit analysis were applied to Soret and α/β bands of WT and DM CYP119 using Fityk software, and a more accurate comparison was obtained.³⁶ The Soret and α/β bands were deconvoluted, and maximum absorbances were obtained from the deconvoluted spectra. The fit of deconvoluted peaks are shown in Figure S2. After analysis, WT CYP119 shows maximum Soret absorbance at 414 nm and the two minor alpha and beta bands at 533 and 568 nm, respectively, similar to previously reported spectra (Figure S2).³⁶ DM CYP119 protein shows a small shift in the Soret maximum to 416 nm, and the α/β bands were observed at 540 and 573 nm (Figure S2).

3.2 | Guaiacol oxidation activity of WT and DM CYP119

Oxidation activity of WT and DM CYP119 was investigated by following the oxidation of guaiacol by H₂O₂ in the presence of enzymes with UV-visible spectroscopy. Reactions contained WT (3 μM) or DM CYP119 (3 μM), guaiacol (5 mM), H₂O₂ (1 mM) in 50 mM potassium phosphate buffer at pH 7.4 and 25°C. During the reaction, an increase at 470 nm can be observed (Figure 1). This band can be attributed to tetraguaiacol formation.³⁸ For WT CYP119, no significant increase in 470 nm was observed (Figure 1); therefore, WT CYP119 does not catalyze guaiacol oxidation. The only change observed in the WT CYP119 reaction is a decrease in the Soret absorbance at 414 nm. Although WT CYP119 does not perform the oxidation reaction for guaiacol substrate, DM CYP119 can catalyze guaiacol oxidation by H₂O₂. At the end of the reaction, 0.13% of guaiacol was oxidized by the DM CYP119, based on the final concentration of tetraguaiacol using the extinction coefficient at

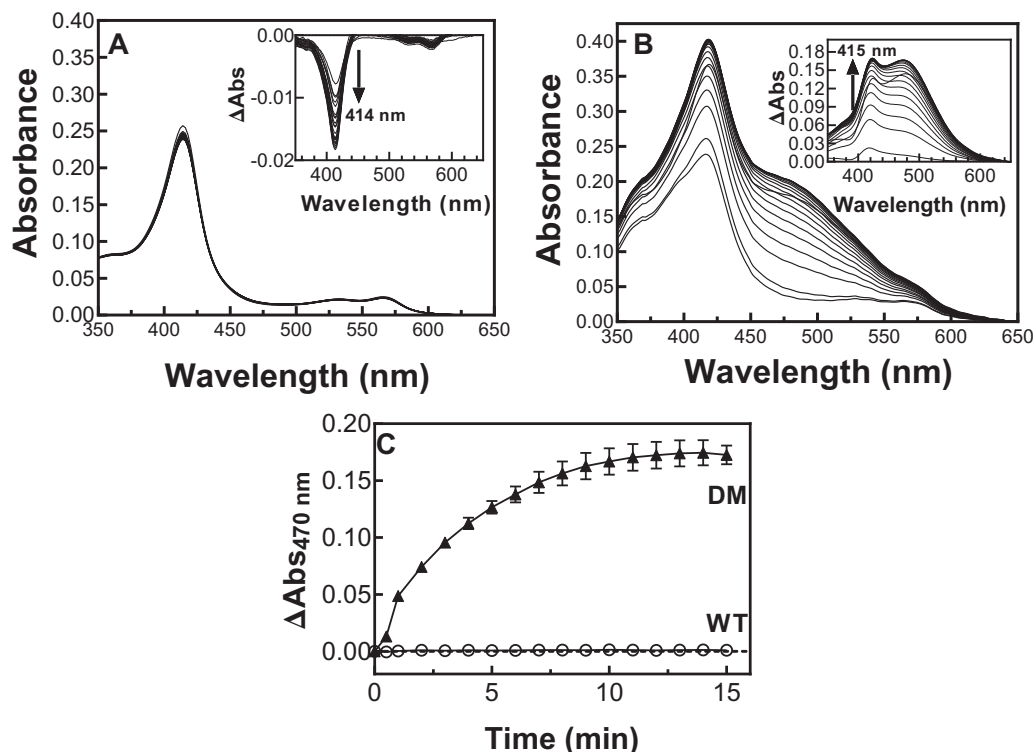


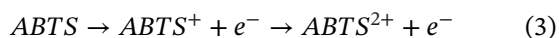
FIGURE 1 Oxidation of guaiacol catalyzed by WT (A) and DM CYP119 (B) in the presence of H_2O_2 . H_2O_2 (1 mM) was added to DM (3 μM) or WT (3 μM) CYP119 and guaiacol (5 mM) in 50 mM potassium phosphate buffer at pH 7.4 and 25°C. The spectra were taken at 1-min intervals for 15 min. Inset: Difference spectra. The product for the reaction, tetraguaiacol shows absorbance at 470 nm during the reaction. Time course of guaiacol oxidation in the presence of WT (O) and DM (◐) CYP119 (C)

470 nm. While the yield of guaiacol oxidation is low under these conditions, it is a significant improvement compared to WT, which does not catalyze the reaction.

3.3 | ABTS oxidation activity of WT and DM CYP119

One electron oxidation of ABTS by WT and DM CYP119 in the presence of H_2O_2 was investigated. The reaction mixtures contained ABTS (1 mM), H_2O_2 (1 mM), WT (1 μM), or DM CYP119 (1 μM) in 50 mM potassium phosphate buffer at pH 7.4. Reaction was monitored at 25°C by UV-visible spectra. $\text{ABTS}^{\bullet+}$ radical cation formation can be observed by a broad band at 734 nm.

We observe that DM CYP119 can catalyze ABTS oxidation by H_2O_2 to generate $\text{ABTS}^{\bullet+}$ radical cation (Figure 2). Absorbance at 734 nm reached maximum after 5 min from the initiation of the reaction with DM CYP119. A decrease in 734 nm was observed after this time; this is thought to be due to oxidation of the $\text{ABTS}^{\bullet+}$ radical by another electron and production of azodication (ABTS^{2+}). This reaction is shown in Equation (3):³⁸



For DM CYP119, maximum $\text{ABTS}^{\bullet+}$ formation was observed at minute 5, at this time 7% of ABTS was oxidized, based on the final concentration of $\text{ABTS}^{\bullet+}$ using the extinction coefficient at 734 nm. On the other hand, WT CYP119 did not catalyze the reaction.

3.4 | Reaction of DM and WT CYP119 with peroxides

H_2O_2 is an important oxidant that is used in peroxygenation reactions. However, most P450s do not utilize H_2O_2 efficiently.³¹ Previous studies demonstrated that WT and DM CYP119 show peroxidation activity in the presence of H_2O_2 . In the absence of substrates, DM CYP119 was more stable toward H_2O_2 degradation compared to WT.³⁴ Here, the effect of other peroxides like CHP and TBHP on WT and DM CYP119 was investigated in the absence of substrates.

WT (1.5 μM) or DM CYP119 (1.5 μM) reacted with CHP or TBHP (1.5 mM) in 50 mM potassium phosphate buffer at 25°C, and changes in the heme Soret absorbance were observed for 45 min by UV-visible spectroscopy during the reaction. Reaction of WT CYP119 with CHP showed a rapid decrease in the Soret absorbance at 414 nm (Figure 3).

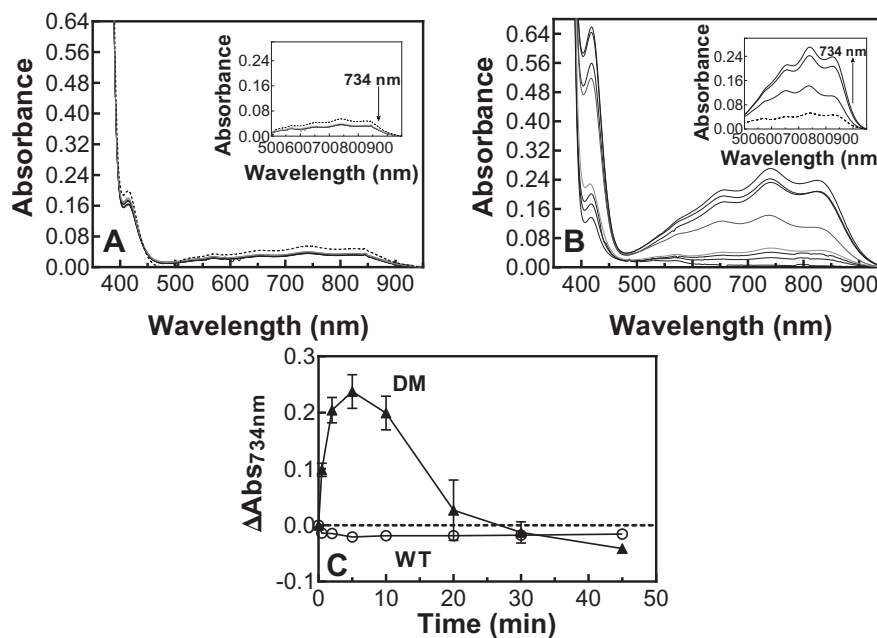


FIGURE 2 Oxidation of ABTS catalyzed by WT and DM CYP119 in the presence of H_2O_2 . Reaction contained WT ($1\ \mu\text{M}$, A) or DM CYP119 ($1\ \mu\text{M}$, B), H_2O_2 (1 mM), ABTS (1 mM) in 50 mM potassium phosphate buffer at 25°C and pH 7.4. The spectra were taken between 350 and 950 nm at 0, 0.5, 2, 5, 10, 20, 30, and 45 min. Inset: Difference spectra. Production of $\text{ABTS}^{+\cdot}$ was monitored by absorbance at 734 nm during the reaction (C). Time course of ABTS oxidation in the presence of WT (O) and DM CYP119 (\blacktriangle)

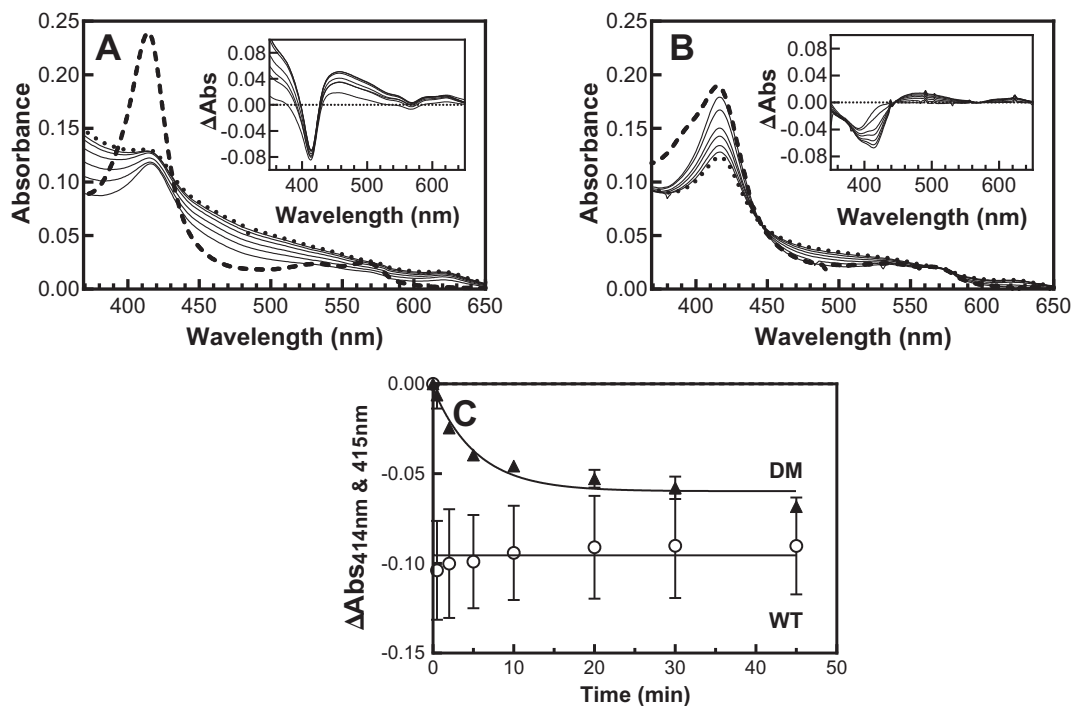


FIGURE 3 Reaction of CHP with WT (A) and DM CYP119 (B) observed by UV-visible spectra. Spectra were taken at 0 (*dashed line*), 2, 5, 10, 20, 30, and 45 min (*dotted line*). Inset shows difference spectra. Reactions involved 1.5 mM H_2O_2 and 1.5 μM enzyme in 50 mM potassium phosphate buffer at pH 7.4. (C) Decrease in 414 nm for WT (O) and DM (\blacktriangle) CYP119

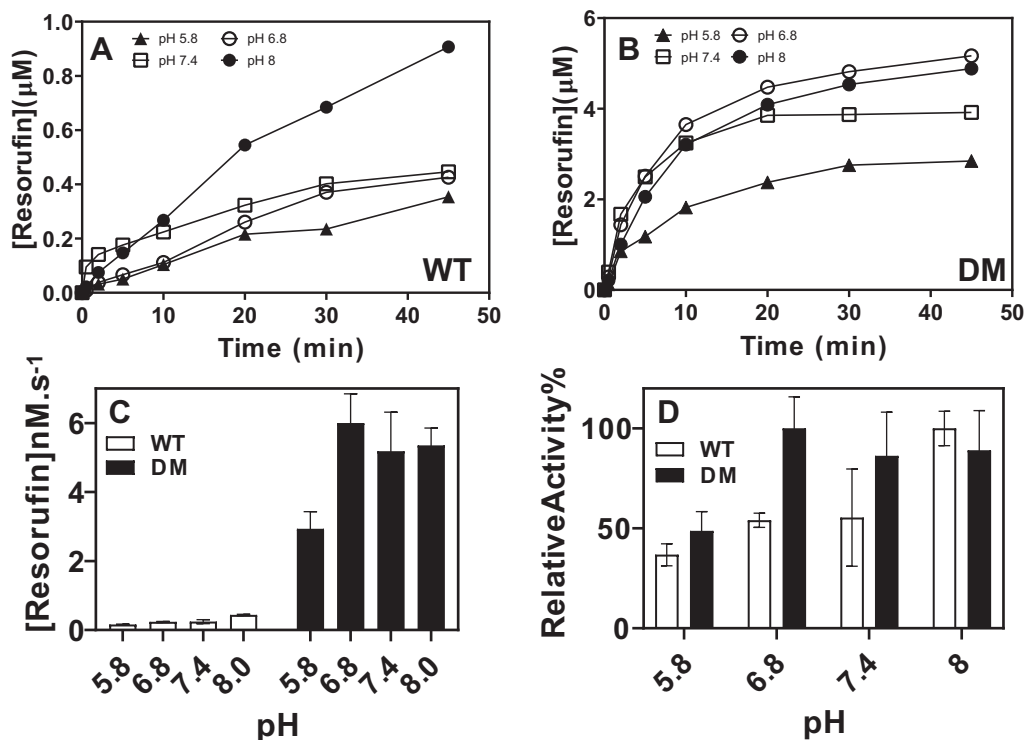


FIGURE 4 Resorufin formation in the presence of WT CYP119 (A) and DM CYP119 (B) at various pH values are illustrated. Initial rate of Amplex Red peroxidation at different pHs are shown. The initial rate of Amplex Red (10 μM) oxidation catalyzed by WT (1.5 μM) and DM CYP119 (1.5 μM) in the presence of H_2O_2 (1.5 mM) in 50 mM potassium phosphate buffer with variable pHs (C). Relative activity normalized for the maximum activity observed for that enzyme for WT and DM CYP119 are shown (D)

At the end of the reaction, the Soret absorbance of WT CYP119 decreased by 42% for CHP and 66% for TBHP (Figures S3 and S4). In addition, an increase in the absorbance at lower wavelengths was observed for WT CYP119 due to aggregation of apoenzyme during the reaction with CHP (Figure 3A). The decrease in Soret absorbance at the end of the reaction (414 nm for WT and 415 nm for DM) in the presence of peroxides (CHP, TBHP, and H_2O_2) are displayed in Figure S4. While TBHP shows the strongest effect on destruction of the heme of both enzymes, CHP and H_2O_2 show intermediate- and low-level effect (Figure S4). The observed rate constant for the decrease in Soret absorbance of WT CYP119 for the decrease in Soret absorbance was 1.2 s^{-1} for CHP, 0.46 s^{-1} for TBHP.

The reactions of DM CYP119 with CHP and TBHP were also monitored by UV-visible spectra (Figure 3 and Figure S3). The Soret absorbance of DM CYP119 at 415 nm decreases by 37% for CHP and by 19% for TBHP. The observed rate constant for the decrease in Soret absorbance of DM CYP119 during the reaction was $3 \times 10^{-3} \text{ s}^{-1}$ for CHP and 0.7 s^{-1} for TBHP.

3.5 | pH profile of Amplex Red peroxidation for DM and WT CYP119

Amplex Red peroxidation activity of WT and DM CYP119 at variable pHs (5.8, 6.8, 7.4, 8) in the presence of H_2O_2 was investigated. The amount of resorufin product formation was measured by using its extinction coefficient at 570 nm. Resorufin formations of WT and DM CYP119 at various pH values are shown in Figure 4. Initial rate of resorufin formation was calculated by linear fitting of resorufin formation with time for the first 10 min of the reaction. Relative activity of WT and DM CYP119 was based on the initial rate. The lowest peroxidation activity for both WT and DM CYP119 was observed at pH 5.8. Peroxidation activity of WT CYP119 increases with increasing pH in the pH range tested. The highest peroxidation activity of WT CYP119 was observed at pH 8. On the other hand, peroxidation activity of DM CYP119 does not change significantly between pH 6.8 and pH 8.0 (Figure 4). In acidic pH, DM shows significantly higher peroxidation activity than WT CYP119 (Figure 4). The highest peroxidation activity for DM CYP119 was observed at pH 6.8.

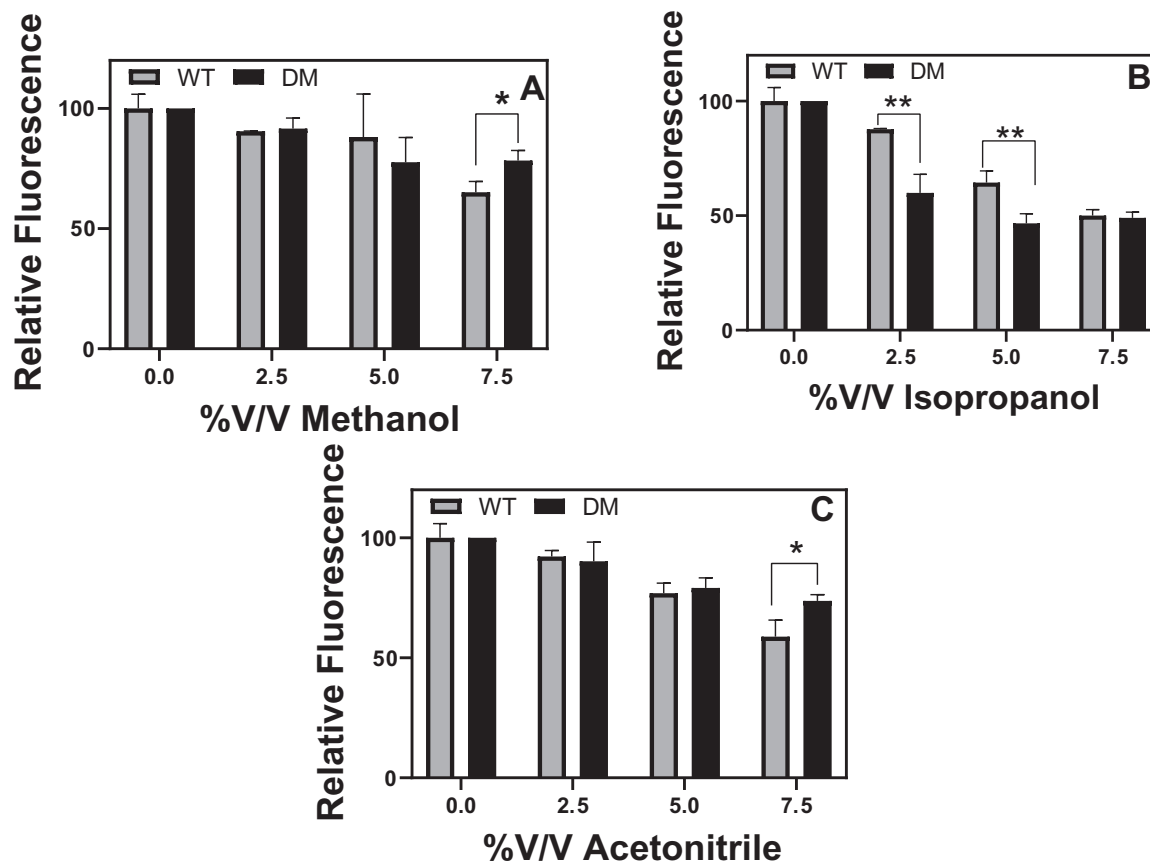


FIGURE 5 Screening of organic solvent effects on peroxidation activity of WT CYP119 (WT; gray) and DM CYP119 (DM; black) were analyzed. Reactions contained variable concentrations of (2.5% v/v, 5% v/v, 7.5% v/v) methanol (A), isopropanol (B), and acetonitrile (C), 1.5 μ M WT CYP119 and DM CYP119, 1.5 mM H_2O_2 , and 10 μ M Amplex Red in 50 mM buffer at pH 7.4. Positive control (PC; reaction without organic solvent). * $p < 0.05$ and ** $p < 0.01$ by a two-tailed unpaired Student's *t*-test

3.6 | Solvent tolerance of WT and DM CYP119

In this study, the effects of methanol, isopropanol and acetonitrile on peroxidation activity of WT and DM CYP119 were investigated. Organic solvents were applied to WT and DM CYP119 at 2.5% v/v, 5% v/v and 7.5% v/v concentrations. Inhibitory effect of organic solvents on WT and DM CYP119 were analyzed.

Peroxidation activity of WT and DM CYP119 were only weakly inhibited (~10% inhibition) at 2.5% v/v methanol. In the presence of 7.5% v/v methanol, inhibition of peroxidation activity of WT (35%) is higher than DM CYP119 (22%) (Figure 5A).

Peroxidation activity was also investigated in the presence of isopropanol. In the presence of 2.5% v/v isopropanol, 13% and 40% inhibition were observed for WT and DM CYP119, respectively. Isopropanol inhibited peroxidation activity at lower concentrations for DM CYP119 compared to WT CYP119. Approximately 50% inhibition of peroxidation activity of WT and DM CYP119 was observed at 7.5% v/v (Figure 5B).

Peroxidation activity was also investigated in the presence of acetonitrile. Approximately 10% inhibition of peroxidation activity was observed in the presence of 2.5% v/v acetonitrile for WT and DM CYP119. In the presence of 7.5% v/v acetonitrile, 26% and 32% inhibition were observed for WT and DM CYP119, respectively (Figure 5C).

3.7 | Temperature stability of WT and DM CYP119

Temperature stability of WT and DM CYP119 was investigated by following Soret absorbance with temperature. WT (3.5 μ M) or DM CYP119 (3.5 μ M) were incubated in 50 mM potassium phosphate buffer for 5 min at each temperature in a dry bath. The changes in Soret absorbance of the enzymes at different temperatures are shown in Figure 6. In addition to the loss of heme cofactor, which leads to decrease in Soret absorbance, at higher temperatures unfolding of the enzymes causes aggregation of apoprotein (Figure 6), which can be observed by the increase in absorbance at lower wavelengths.

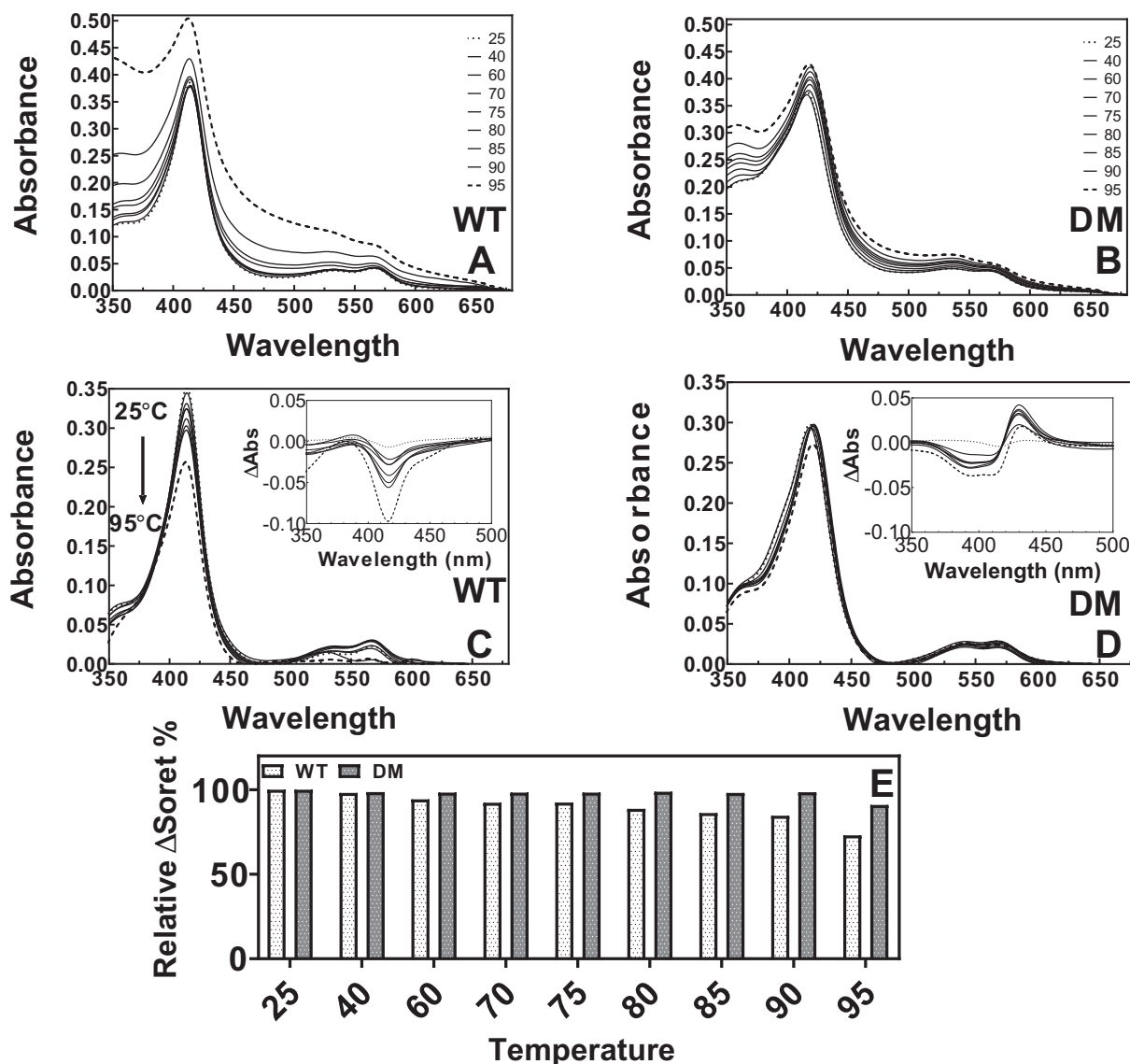


FIGURE 6 UV-visible spectra of thermostability analysis of raw data of $3.5 \mu\text{M}$ WT CYP119 (A) and subtract data of WT CYP119 (C) are shown. UV-visible spectra of thermostability analysis of raw data of $3.5 \mu\text{M}$ DM CYP119 (B) and subtract data (D) of DM CYP119 are shown (25°C [dotted line], 95°C [dashed line]). Insets: Difference absorption spectra of thermostability analysis of WT (C) and DM CYP119 (D) (40°C [dotted line], 95°C [dashed line]). Relative Soret absorbance at recorded temperature compared to absorbance at room temperature of WT ($3.5 \mu\text{M}$) and DM CYP119 ($3.5 \mu\text{M}$) are illustrated at selected temperatures (25°C , 40°C , 60°C , 70°C , 75°C , 80°C , 85°C , 90°C , and 95°C) (E)

Decrease of maximum Soret absorbance (27%) of WT CYP119 was observed due to denaturation and loss of heme from the protein. Difference spectra demonstrate a significant decrease at 416 nm (Figure 6C inset). When the effects of increased temperature on DM CYP119 were analyzed based on difference spectrum, a shift maximum Soret absorbance was observed from 433 to 395 nm. The Soret absorbance of DM CYP119 was decreased by 9% at 95°C (Figure 6D and inset). As seen in Figure 6A, aggregation of apoprotein resulted in significant changes in the UV-visible spectra, especially for WT CYP119. To correct for scattering at lower wavelengths due to protein aggregation, background subtraction by Fityk1.3.1 was applied to all

spectra (Figure 6).³⁵ After background subtraction, relative decrease in Soret absorbance of WT CYP119 with increasing of temperature was more clearly observed, as seen in Figure 6E.

3.8 | Substrate scope of WT versus DM

To elucidate the differences in substrate specificity among the WT and DM CYP119 and to provide a consensus on which of the enzymes show preference for ligand binding, molecular docking of substrates was performed on the active sites of WT and DM CYP119. The substrates tested



TABLE 1 Docking energy scores of substrates are illustrated for WT (1F4T) and DM CYP119

Substrate	Docking score (REU)	
	WT CYP119	DM CYP119
Caffeine	−418	−1195
Testosterone	−516	−1176
Progesterone	−412	−1119
Amplex Red	−517	−1185
Guaiacol	−441	−1205
Phenoxazine	−528	−1209
Indole	−409	−1207
Indoxyl acetate	−446	−1149
SDS	−441	−1178

were Amplex Red, guaiacol, progesterone, testosterone, caffeine, SDS, indole, and indoxyl acetate and phenoxazine (Figure S5). One hundred rounds of ligand docking were performed for both WT CYP119 and the DM CYP119. Score distribution histograms for docking results are shown in Figures S6–S8. Scoring function of PyRosetta occurs in a composition of physics-based and knowledge-based information about the structure, thus the energy scores were calculated as a generic unit (REU).⁴¹ When the docking models were examined, the most negative REU scores were approved as more native-like.⁴¹ The lowest REU scores were chosen to determine ligand–protein interactions (Table 1). To understand differences of substrate diversity of WT and DM CYP119, the volume surface of binding pocket of enzymes were also calculated as 331 Å³ and 267 Å³, respectively, by Castp analysis.⁴² The surface of binding pocket of WT (PDB: 1F4T) and DM CYP119 are displayed in Figure S9.

Docking scores and the distance of the ligands from the heme group were investigated to predict binding affinity and oxidation of the enzymes, respectively. Ligand docking of guaiacol molecule into the WT (PDB ID: 1F4T) and DM CYP119 was performed by using the PyRosetta program (Figure S10). For WT CYP119, the guaiacol demonstrates low binding affinity with selected lowest score from docking results (−441 REU). The distance between the heme iron atom and the targeted carbon atom of guaiacol was measured as 4.5 Å for WT CYP119. For DM CYP119, the guaiacol displayed a relatively high binding ability with the lowest score (−1205 REU, Table 1), and the distance between the heme iron atom and the targeted carbon atom of guaiacol was measured as 3.78 Å.

Ligand docking of progesterone molecule into the WT (PDB ID: 1F4T) and DM CYP119 was performed by using the PyRosetta program (Figure S11). For WT CYP119, progesterone demonstrated low binding ability with the lowest score from docking results being −412 REU (Table 1).

The distance between the heme iron atom and the targeted carbon atom of progesterone was measured as 2.5 Å for WT CYP119. For DM CYP119, the progesterone displayed a relatively high binding ability with a more negative lowest score (−1119 REU, Table 1), and the distance between the heme iron atom and the targeted carbon atom of guaiacol was measured as 2.4 Å.

3.9 | Progesterone binding and conversion with WT and DM CYP119

As docking studies indicated that DM CYP119 has higher affinity for progesterone, its affinity for WT and DM CYP119 was studied. Upon binding of progesterone to WT or DM CYP119, a shift in spin state equilibrium toward high spin to low spin is observed, which results in a decrease in absorbance at 388 nm and increase in absorbance at 420 nm (Figure 7). The K_d values for both of enzymes were obtained from analysis of the shift in Soret absorbance using Equation 2. WT CYP119 showed 250-fold lower affinity for progesterone ($K_d = 18,000 \pm 7300 \mu\text{M}$) compared to DM CYP119 ($K_d = 71 \pm 17 \mu\text{M}$).

Conversion of progesterone by WT and DM CYP119 using CHP as an oxidant was investigated (Figure S12). Reactions contained WT (10 μM) or DM CYP119 (10 μM), progesterone (150 μM), CHP (1 mM) in 50 mM potassium phosphate buffer at pH 7.4 and 25°C. Products of reaction were extracted and analyzed by HPLC. Figure S12 shows representative chromatograms of the progesterone metabolites formed by WT and DM CYP119. HPLC chromatogram was followed at 254 nm for detection of products (Figure S12). Retention time of progesterone was detected at 14.7 min and retention times of CHP only products were detected at 7.1, 8.3, and 9.2 min. A new product peak at 10.5 min was observed in presence of DM CYP119. This peak was not observed in control reaction and in the reaction by WT CYP119 (Figure S12).

4 | DISCUSSION

P450s has tremendous potential for biotechnological use, no other enzyme family has such a vast variety of substrates and the types of reactions they catalyze. However, compared to widely applied commercial enzymes, their practical applications are limited due to the disadvantages of the P450 systems. Low stability, low solubility, narrow substrate scope, expensive cofactors, dependence on redox partners, and low substrate solubility of P450s severely limit broader application of these enzymes.⁹ Here, we characterize a novel CYP119 variant (T213R/T214I, DM) that addresses most of these limitations observed in P450s.

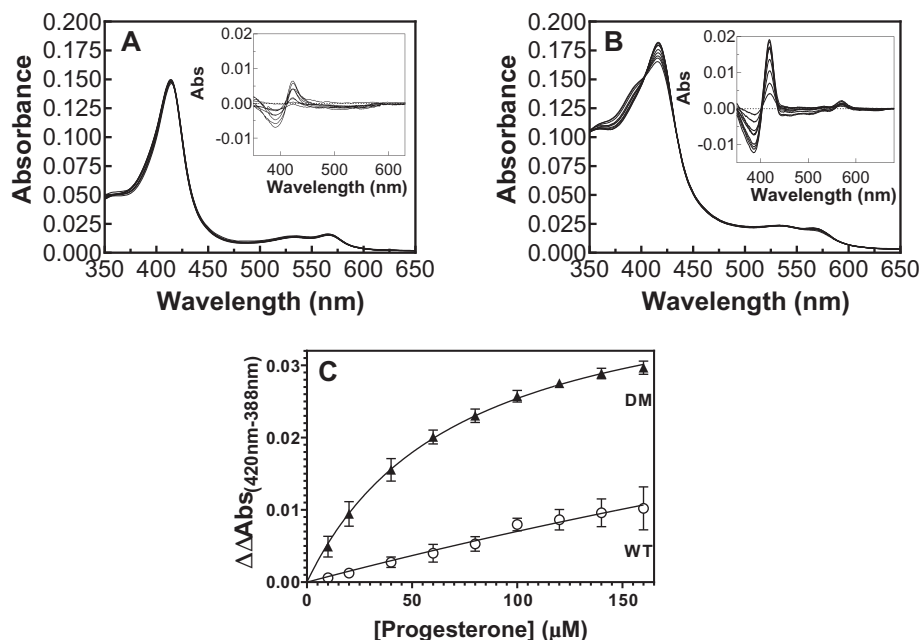


FIGURE 7 UV-visible and difference spectra of WT (A) DM CYP119 (B) titrated with saturated progesterone. Overlay of UV-visible spectra of 1.5 μM WT CYP119 or DM CYP119 with different concentrations of progesterone (0.01–160 μM). The insets show difference spectra with increasing progesterone concentrations. (C) The absorbance shifts observed in 420 and 388 nm for progesterone binding titration of WT (O) and DM CYP119 (\blacktriangle). The absorbance difference between 420 and 388 nm ($\Delta\Delta\text{Abs}$ [420 – 388 nm]) versus concentrations of progesterone plotted by nonlinear fitting

We show that DM CYP119 is a soluble thermophilic P450, with a broad substrate specificity that does not require expensive cofactors and redox partners in its reactions.

DM CYP119 was obtained through a high-throughput screen of CYP119 mutants for Amplex Red oxidation activity using H_2O_2 as an oxidant.³⁴ Therefore, it showed five-fold increased activity and higher affinity for Amplex Red. In addition, DM CYP119 catalyzed styrene epoxidation with two-fold increased activity compared to WT. However, its activity toward other substrates has not been tested. Here, we show that DM CYP119 can also oxidize guaiacol and ABTS, while WT CYP119 shows no detectible activity with these substrates (Figures 1 and 2). Increased activity of DM CYP119 toward these unnatural substrates led us to investigate the catalytic promiscuity of this enzyme by docking potential substrates to the modeled DM CYP119 active site. Nine potential substrates including bioactive compounds such as caffeine, indole, testosterone, and progesterone were screened by docking simulations; all these compounds showed increased affinity for DM CYP119 compared to WT based on Rosetta score function (Table 1).

Based on PyRosetta docking results, DM CYP119, which has lower REUs (Table 1), is predicted to have higher affinity to the molecules tested. However, it is not possible to obtain binding energies directly for these ligands by using PyRosetta. PyRosetta has a class of scoring func-

tions, which contains a combination of physics-based and knowledge-based information about structure, and also statistical parameters.⁴³ Because some parameters of Rosetta score function (van der Waals energy scores, attraction and repulsion values, hydrogen and covalent bonds, etc.) has the kcal/mol as unit, a correlation between REU scores and kcal/mol scores might be expected, but so far there is no experimental validation done to confirm that.⁴⁴ To obtain an estimate of binding energies, docking of ligands into WT and DM CYP119 was also performed by Chimera with AutoDock vina, which outputs energy scores in kcal/mol (Figure S13). Docking results obtained by PyRosetta and Chimera were consistent (Figure S13). Based on Chimera results, binding energies were in the -7.4 to -4.5 kcal/mol range for DM CYP119 and in the -0.6 to $+3.9$ kcal/mol range for WT (Figure S13). PyRosetta and Chimera have different assumptions for binding energy calculations, so docking scores of some molecules (indole and guaiacol) could not be obtained by Chimera.

Among the compounds that were predicted to have a higher affinity for DM CYP119, progesterone is of particular interest by the pharmaceutical industry, as hydroxylated progesterone derivatives can play physiological roles and can be intermediates in the synthesis of other steroid-based drugs. Therefore, affinity of DM and WT CYP119 for progesterone was also determined experimentally. DM CYP119 showed 250-fold increased

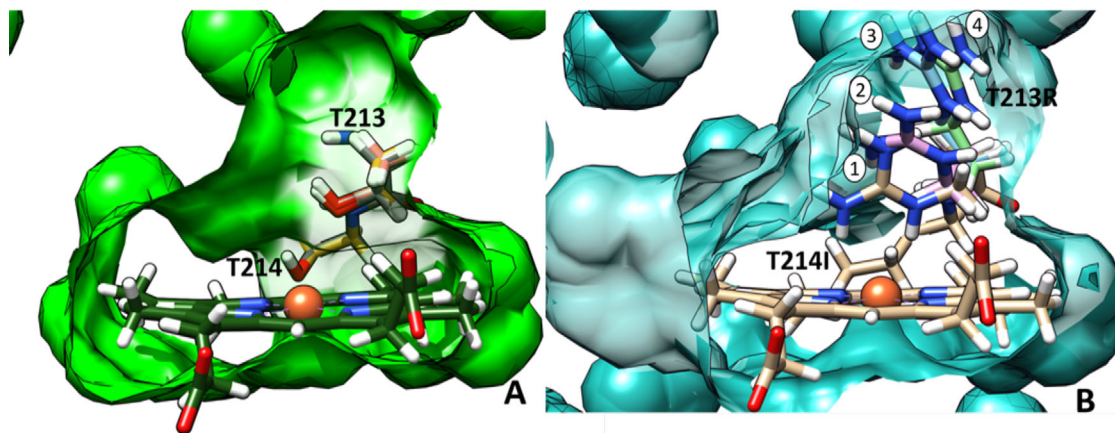


FIGURE 8 Substrate binding cavity and mutated residues of WT (PDB code 1F4T, A [12]) and DM CYP119 (B) after docking various substrates is shown. The side chain conformation of T213R depends on the docking. Different conformations of Arg213 with: (1) Amplex Red, caffeine, and SDS; (2) phenoxazine; (3) indole and guaiacol; (4) progesterone, testosterone, and indoxyl acetate. No significant conformational change was observed in WT CYP119 Thr213 residue after docking with different substrates

affinity for progesterone confirming the computational analysis. In addition, DM CYP119 catalyzed formation of a new product in oxidation progesterone with CHP (Figure S12). Future studies are necessary to optimize the product formation and identify the new product.

To understand the broad substrate specificity of DM CYP119, the substrate binding pockets of WT and DM CYP119 were investigated. The molecular size of Arg (173.4 \AA^3) is larger than that of Thr (116.1 \AA^3)⁴⁵; therefore, as expected the substrate binding pocket of DM CYP119 (267 \AA^3) was smaller than that of WT (331 \AA^3), as calculated by Castp (Figure S9).⁴² On the other hand, larger substrates like Amplex Red and progesterone still showed higher affinity for DM CYP119. This can be explained by the different conformations of the side chains in the mutated residues especially Arg213 in the enzyme–substrate complex. The side chain of Arg213 in DM CYP119 shows increased flexibility and interacts with a variety of substrates at different positions as seen in the docking results (Figure 8). The active sites of DM and WT CYP119 are compared in Figure 8, which shows the flexibility of the arginine residue.

Most P450s utilize the reductive oxygen activation pathway for their reactions. On the other hand, H_2O_2 -shunt pathway does not require any expensive cofactors or electron transfer proteins. In addition, the low cost of H_2O_2 makes peroxide utilizing P450s attractive targets for industrial-scale synthesis. DM CYP119 was developed for increased efficiency with H_2O_2 and showed increased activity with reactions using H_2O_2 as oxidant. Peroxide-shunt pathway can also be supported by CHP and TBHP. However, reactions with peroxides also lead to “suicide inactivation” where the participating P450 is sacrificed due to destruction of the essential prosthetic heme group.⁴⁶

Stability of the heme group against degradation by peroxides will lead to increased enzyme activity and increased yield in the presence of peroxides. Previously, we showed that DM CYP119 was more resistant to heme degradation by H_2O_2 . Here, we tested the stability of DM CYP119 against other commonly used peroxides like CHP and TBHP. DM CYP119 showed increased stability against all peroxides tested (Figure 3 and Figures S3 and S4). Heme degradation occurred slower and to a lower extent in DM CYP119 compared to WT.

The reason for the stability of DM CYP119 against peroxide-dependent degradation can be due to less accessible heme pocket with larger arginine residue blocking the heme cofactor. However, this is not consistent with higher H_2O_2 -supported activity by DM CYP119. X-ray crystal structure analyses of heme-containing enzymes indicate that the presence of residues that can support acid–base catalysis at the distal heme pocket can enhance the generation of the reactive intermediate compound I and stabilize it.²³ Indeed, distal arginine residues play important roles in the reactions of HRP and P450bs β with peroxidases. However, in both cases the arginine cooperates with another basic group (histidine residue in HRP and carboxylate group of the substrate in P450bs β).⁴⁷ Analysis of the structure of DM CYP119 did not reveal such a basic group near the distal pocket. As the distal pocket of DM CYP119 is significantly more hydrophilic than WT (Figure S9), a distal water molecule may assist Arg213 in catalysis.

The effect of pH on the initial rate of Amplex Red peroxidation of WT and DM CYP119 was also investigated. In accordance with previous results for WT CYP119 activity increased with pH and reached maximum at pH 8.0 (Figure 4).¹ In addition, there was approximately 50% decrease in activity at pH 6.8 compared to pH 8.0.

On the other hand, for DM CYP119 the initial rate did not change significantly between pH 6.8 to pH 8.0. DM CYP119 shows high activity in a relatively large range of pH values, which will increase its industrial applications.

As CYP119 is obtained from an acidothermophilic organism, it is a thermostable protein. Previous studies have determined the melting temperature (T_m) of WT CYP119 as 91°C using differential scanning calorimetry.² Here, the Soret absorbance was followed to determine heme loss and aggregation with increasing temperature. There was no significant decrease in Soret absorbance for WT CYP119 between 20°C and 80°C (Figure 6). This is consistent with previous observations, which did not observe a significant change in heme chromophore or styrene epoxidation activity of WT CYP119 between these temperatures.²⁸ DM CYP119 showed even higher relative Soret absorbance with increasing temperature (Figure 6); therefore, it has at least similar thermostability to WT CYP119. We note that previous results for WT CYP119 have shown a significant drop in heme chromophore at 90°C, which is not observed under our experimental conditions.²⁸ The difference observed at this temperature likely arises from incubation time, which was shorter in our assay.

The stability of enzymes in organic solvents is an important problem in biocatalysis, especially in the synthesis of fine chemicals and pharmaceuticals. Increasing enzyme tolerance to organic solvents will allow for an increase in concentration of insoluble substrates and products that can be employed, which will lead to a wider range of operating conditions.⁴⁸ Previous studies indicate that proteins stable at higher temperatures also show stability in the presence of organic solvents.^{27,49} Because WT and DM CYP119 show increased thermostability, we tested their peroxidase activity in the presence of commonly used organic solvents, such as methanol, acetonitrile, and isopropanol (Figure 5). As expected, WT CYP119 does not show significant inactivation in the presence of organic solvents, it retains ~70% of its activity in the presence of 7.5% v/v acetonitrile. In comparison, WT P450-BM3 (CYP102) only retains 20% of its activity under the same conditions.⁵⁰ DM CYP119 shows similar inactivation levels with lower concentrations of acetonitrile and methanol (Figure 5). On the other hand, at the highest concentrations (7.5% v/v) tested of acetonitrile and methanol, DM shows lower inhibition for these solvents compared to WT. Therefore, T213R/T214I mutation might confer slightly higher stability in the presence of these solvents. Among the solvents tested, methanol demonstrates the lowest inhibitory effect for peroxidation activity of both WT and DM CYP119. On the other hand, DM CYP119 seems to be sensitive to isopropanol, especially at low concentrations. At 2.5% and 5% v/v isopropanol, DM is significantly more inhibited than WT CYP119

(Figure 5B). The reason for this sensitivity is currently unclear; isopropanol may have specific interactions with the active site.

In conclusion, T213R/T214I (DM) CYP119 can serve as a useful biocatalyst for industrial applications: it is a soluble enzyme that has a broad substrate scope, shows relatively high activity with peroxidases, it is thermostable and stable against degradation by peroxidases, and shows tolerance of the catalytic activity to organic solvents. The peroxidase activity of DM CYP119 shows broad pH tolerance compared to WT CYP119, this could prove useful not only in industrial applications but also in mechanistic studies. The high tolerance of DM CYP119 to cosolvents is a particularly useful feature for pharmaceutical industry, as selective oxidation of hydrophobic molecules with poor water solubility is a necessity. DM CYP119 can also be a good starting point for further directed evolution studies to increase substrate selectivity or further increase peroxidase-dependent activity. Combining further protein engineering approaches to the already attractive features of DM CYP119—peroxidase activity, broad substrate scope, thermostability, and solvent tolerance—will lead to extending the application of this protein in several fields of biotechnology.


ACKNOWLEDGMENTS

We thank Çağlar Karakaya for allowing access to ultrasonic instrument. We are grateful to İzmir Institute of Technology, Biology and Bioengineering Applications and Research Center (BIYOMER) for allowing use of HPLC instrument. We also thank Melis Küçüksoğak and Gülce Güralp for their help with the HPLC analysis.

CONFLICT OF INTEREST

The authors declare that there is no conflict of interest.

ORCID

Nur Basak Surmeli  <https://orcid.org/0000-0002-1841-4004>

REFERENCES

1. Rabe KS, Kiko K, Niemeyer CM. Characterization of the peroxidase activity of CYP119, a thermostable P450 from *Sulfolobus acidocaldarius*. *ChemBioChem*. 2008;9:420–5.
2. McLean MA, Maves SA, Weiss KE, Krepich S, Sligar SG. Characterization of a cytochrome P450 from the acidothermophilic archaea *Sulfolobus solfataricus*. *Biochem Biophys Res Commun*. 1998;252:166–72.
3. Omura T. Recollection of the early years of the research on cytochrome P450. *Proc Jpn Acad Ser B Phys Biol Sci*. 2011;87:617–40.
4. Rabe KS, Erkelenz M, Kiko K, Niemeyer CM. Peroxidase activity of bacterial cytochrome P450 enzymes: modulation by fatty acids and organic solvents. *Biotechnol J*. 2010;5:891–9.



5. Rabe KS, Gandubert VJ, Spengler M, Erkelenz M, Niemeyer CM. Engineering and assaying of cytochrome P450 biocatalysts. *Anal Bioanal Chem.* 2008;392:1059–73.
6. Sakaki T. Practical application of cytochrome P450. *Biol Pharm Bull.* 2012;35:844–9.
7. Di Nardo G, Gilardi G. Natural compounds as pharmaceuticals: the key role of cytochromes P450 reactivity. *Trends Biochem Sci.* 2020;45:511–25.
8. Zhang X, Guo J, Cheng F, Li S. Cytochrome P450 enzymes in fungal natural product biosynthesis. *Nat Prod Rep.* 2021;38:1072–99.
9. Li Z, Jiang Y, Guengerich FP, Ma L, Li S, Zhang W. Engineering cytochrome P450 enzyme systems for biomedical and biotechnological applications. *J Biol Chem.* 2020;295:833–49.
10. Bernhardt R, Urlacher VB. Cytochromes P450 as promising catalysts for biotechnological application: chances and limitations. *Appl Microbiol Biotechnol.* 2014;98:6185–203.
11. Park SY, Yamane K, Adachi SI, Shiro Y, Weiss KE, Maves SA, et al. Thermophilic cytochrome P450 (CYP119) from *Sulfolobus solfataricus*: high resolution structure and functional properties. *J Inorg Biochem.* 2002;91:491–501.
12. Matthews S, Belcher JD, Tee KL, Girvan HM, McLean KJ, Rigby SE, et al. Catalytic determinants of alkene production by the cytochrome P450 peroxygenase OleTJE. *J Biol Chem.* 2017;292(12):5128–143. <https://doi.org/10.1074/jbc.m116.762336>
13. Hammerer L, Friess M, Cerne J, Fuchs M, Steinkellner G, Gruber K, et al. Controlling the regioselectivity of fatty acid hydroxylation (C10) at α - and β -position by CYP152A1 (P450Bs β) variants. *ChemCatChem.* 2019;11(22):5642–649. <https://doi.org/10.1002/cctc.201901679>
14. Ciaramella A, Catucci G, Di Nardo G, Sadeghi SJ, Gilardi G. Peroxide-driven catalysis of the heme domain of A. radiorensistens cytochrome P450 I16B5 for sustainable aromatic rings oxidation and drug metabolites production. *N Biotechnol.* 2020;54:71–9.
15. Ciaramella A, Catucci G, Gilardi G, Di Nardo G. Crystal structure of bacterial CYP116B5 heme domain: new insights on class VII P450s structural flexibility and peroxygenase activity. *Int J Biol Macromol.* 2019;140:577–87.
16. Fürst MJLJ, Kerschbaumer B, Rinnofner C, Migglautsch AK, Winkler M, Fraaije MW. Exploring the biocatalytic potential of a self-sufficient cytochrome P450 from *thermothelomyces thermophila*. *Adv Synth Catal.* 2019;361:2487–96.
17. Kumar S, Sun L, Liu H, Muralidhara BK, Halpert JR. Engineering mammalian cytochrome P450 2B1 by directed evolution for enhanced catalytic tolerance to temperature and dimethyl sulfoxide. *Protein Eng Des Sel.* 2006;19:547–54.
18. Xu J, Wang C, Cong Z. Strategies for substrate-regulated P450 catalysis: from substrate engineering to co-catalysis. *Chem Eur J.* 2019;25:6853–63.
19. Shoji O, Fujishiro T, Nakajima H, Kim M, Nagano S, Shiro Y, et al. Hydrogen peroxide dependent monooxygenations by tricking the substrate recognition of cytochrome P450BSbeta. *Angew Chem Int Ed.* 2007;46:3656–9.
20. Ma N, Chen Z, Chen J, Chen J, Wang C, Zhou H, et al. Dual-functional small molecules for generating an efficient cytochrome P450BM3 peroxygenase. *Angew Chem Int Ed.* 2018;57:7628–33.
21. Matsumura H, Wakatabi M, Omi S, Ohtaki A, Nakamura N, Yohda M, et al. Modulation of redox potential and alteration in reactivity via the peroxide shunt pathway by mutation of cytochrome P450 around the proximal heme ligand. *Biochemistry.* 2008;47:4834–42.
22. Hayakawa S, Matsumura H, Nakamura N, Yohda M, Ohno H. Identification of the rate-limiting step of the peroxygenase reactions catalyzed by the thermophilic cytochrome P450 from *Sulfolobus tokodaii* strain 7. *FEBS J.* 2014;281:1409–16.
23. Behera RK, Goyal S, Mazumdar S. Modification of the heme active site to increase the peroxidase activity of thermophilic cytochrome P450: a rational approach. *J Inorg Biochem.* 2010;104:1185–94.
24. Joo H, Lin Z, Arnold FH. Laboratory evolution of peroxide-mediated cytochrome P450 hydroxylation. *Nature.* 1999;399(6737):670–73. <http://doi.org/10.1038/21395>
25. Matsuura K, Toshi T, Yoshioka S, Takahashi S, Ishimori K, Morishima I. Structural and functional characterization of "laboratory evolved" cytochrome P450cam mutants showing enhanced naphthalene oxygenation activity. *Biochem Biophys Res Commun.* 2004;323:1209–15.
26. Yano JK, Koo LS, Schuller DJ, Li H, Ortiz de Montellano PR, Poulos TL. Crystal structure of a thermophilic cytochrome P450 from the archaeon *Sulfolobus solfataricus*. *J Biol Chem.* 2000;275:31086–92.
27. Cowan DA. Thermophilic proteins: stability and function in aqueous and organic solvents. *Comp Biochem Physiol A Physiol.* 1997;118:429–38.
28. Koo LS, Tschirret-Guth RA, Straub WE, Moënné-Loccoz P, Loehr TM, Ortiz de Montellano PR. The active site of the thermophilic CYP119 from *Sulfolobus solfataricus*. *J Biol Chem.* 2000;275:14112–23.
29. Brock TD, Brock KM, Belly RT, Weiss RL. *Sulfolobus*: a new genus of sulfur-oxidizing bacteria living at low pH and high temperature. *Arch Mikrobiol.* 1972;84:54–68.
30. Childs RE, Bardsley WG. The steady-state kinetics of peroxidase with 2,2'-azino-di-(3-ethyl-benzthiazoline-6-sulphonic acid) as chromogen. *Biochem J.* 1975;145:93–103.
31. Shoji O, Watanabe Y. Peroxygenase reactions catalyzed by cytochromes P450. *J Biol Inorg Chem.* 2014;19:529–39.
32. de Montellano PRO. *Cytochrome P450. Structure, mechanism, and biochemistry*, 4th ed. Springer International Publishing; 2015. <https://www.springer.com/gp/book/9780306483240>
33. Reetz MT, Bocola M, Carballeira JD, Zha D, Vogel A. Expanding the range of substrate acceptance of enzymes: combinatorial active-site saturation test. *Angew Chem Int Ed.* 2005;44:4192–6.
34. Başlar MS, Sakallı T, Güralp G, Kestevür Doğru E, Haklı E, Surmeli NB. Development of an improved Amplex Red peroxidation activity assay for screening cytochrome P450 variants and identification of a novel mutant of the thermophilic CYP119. *J Biol Inorg Chem.* 2020;25:949–62.
35. Wojdyr M. Fityk: a general-purpose peak fitting program. *J Appl Crystallogr.* 2010;43:1126–8.
36. Aslantas Y, Surmeli NB. Effects of N-terminal and C-terminal polyhistidine tag on the stability and function of the thermophilic P450 CYP119. *Bioinorg Chem Appl.* 2019;2019:8080697.
37. Maehly AC. The assay of catalases and peroxidases. *Methods Biochem Anal.* 1954;1:357–424.

38. Aggrey-Fynn JE, Surmeli NB. A novel thermophilic hemoprotein scaffold for rational design of biocatalysts. *J Biol Inorg Chem*. 2018;23:1295–307.
39. Chaudhury S, Lyskov S, Gray JJ. PyRosetta: a script-based interface for implementing molecular modeling algorithms using Rosetta. *Bioinformatics*. 2010;26:689–91.
40. Pettersen EF, Goddard TD, Huang CC, Couch GS, Greenblatt DM, Meng EC, et al. UCSF Chimera—a visualization system for exploratory research and analysis. *J Comput Chem*. 2004;25:1605–12.
41. Misura KMS, Chivian D, Rohl CA, Kim DE, Baker D. Physically realistic homology models built with ROSETTA can be more accurate than their templates. *Proc Natl Acad Sci U S A*. 2006;103:5361–6.
42. Tian W, Chen C, Lei X, Zhao J, Liang J. CASTp 3.0: computed atlas of surface topography of proteins. *Nucleic Acids Res*. 2018;46:363–7.
43. Song Y, Tyka M, Leaver-Fay A, Thompson J, Baker D. Structure-guided forcefield optimization. *Proteins*. 2011;79:1898–909.
44. Kellogg EH, Leaver-Fay A, Baker D. Role of conformational sampling in computing mutation-induced changes in protein structure and stability. *Proteins*. 2011;79:830–8.
45. Zamyatnin AA. Protein volume in solution. *Prog Biophys Mol Biol*. 1972;24:107–23.
46. de Montellano PRO, Reich NO. Inhibition of Cytochrome P-450 Enzymes. In: de Montellano, editor. *Cytochrome P-450*. Boston, US: Springer; 1986. p. 273–314. https://doi.org/10.1007/978-1-4757-9939-2_8
47. Matsunaga I, Shiro Y. Peroxide-utilizing biocatalysts: structural and functional diversity of heme-containing enzymes. *Curr Opin Chem Biol*. 2004;8:127–32.
48. Dordick JS. Enzymatic catalysis in monophasic organic solvents. *Enzyme Microb Technol*. 1989;11(4):194–211. [https://doi.org/10.1016/0141-0229\(89\)90094-x](https://doi.org/10.1016/0141-0229(89)90094-x)
49. Owusu RK, Cowan DA. Thermostable microbial protein stability in aqueous: organic two-solvent phase systems. *Biochem Soc Trans*. 1989;17:581–2.
50. Wong TS, Arnold FH, Schwaneberg U. Laboratory evolution of cytochrome p450 BM-3 monooxygenase for organic cosolvents. *Biotechnol Bioeng*. 2004;85:351–8.

SUPPORTING INFORMATION

Additional supporting information may be found in the online version of the article at the publisher's website.

How to cite this article: Sakalli T, Surmeli NB. Functional characterization of a novel CYP119 variant to explore its biocatalytic potential. *Biotechnology and Applied Biochemistry*. 2022;69:1741–1756. <https://doi.org/10.1002/bab.2243>